Hydrological effect of vegetation against rainfall-induced landslides

Gonzalez Ollauri, Alejandro; Mickovski, Slobodan B.

Published in:
Journal of Hydrology

DOI:
10.1016/j.jhydrol.2017.04.014

Publication date:
2017

Document Version
Author accepted manuscript

Hydrological effect of vegetation against rainfall-induced landslides

Authors: Alejandro Gonzalez-Ollauri[1,2] and Slobodan B. Mickovski[1]
[1]School of Engineering & Built Environment, Glasgow Caledonian University, Glasgow, UK
[2]Corresponding author: alejandro.ollauri@gcu.ac.uk +44(0)1413313433
SEBE, Glasgow Caledonian University, Cowcaddens Road, G4 0BA Glasgow, UK

Abstract

The hydrological effect of vegetation on rainfall-induced landslides has rarely been quantified and its integration into slope stability analysis methods remains a challenge. Our goal was to establish a reproducible, novel framework to evaluate the hydrological effect of vegetation on shallow landslides. This was achieved by accomplishing three objectives: (i) quantification *in situ* of the hydrological mechanisms by which woody vegetation (i.e. *Salix* sp.) might impact slope stability under wetting and drying conditions; (ii) to propose a new approach to predict plant-derived matric suctions under drying conditions; and (iii) to evaluate the suitability of the *unified effective stress principle* and framework (UES) to quantify the hydrological effect of vegetation against landslides. The results revealed that plant water uptake was the main hydrological mechanism contributing to slope stability, as the vegetated slope was, on average, 12.84% drier and had matric suctions three times higher than the fallow slope. The plant-related mechanisms under wetting conditions had a minimal effect on slope stability. The plant aerial parts intercepted up to 26.73% of the rainfall and concentrated a further 10.78% of it around the stem. Our approach successfully predicted the plant-derived matric suctions and UES proved to be adequate for evaluating the hydrological effect of vegetation on landslides. Although the UES framework presented here sets the basis for effectively evaluating the hydrological effect of vegetation on slope stability, it requires knowledge of the specific hydro-mechanical properties of plant-soil composites and this in itself needs further investigation.

Keywords: hydrological, vegetation, willow, matric suction, landslide, slope stability

1. Introduction

Rainfall-induced landslides are global phenomena that result in loss of human life and damage to property every year (Sidle and Bogaard, 2016). They are normally triggered by a decrease in the soil shear strength after heavy rainfall events on sloped terrain (Lu and Godt, 2013). As a consequence of the predicted intensification of the hydrological cycle due to climate change?? (Roderick et al., 2014), the likelihood of rainfall-induced landslides is expected to increase, making the implementation of mitigation and remediation measures a priority.

Vegetation has been proven to be an effective landslide mitigation measure, as it enhances the soil shear strength via a series of mechanical and hydrological effects (Norris et al., 2008). While the mechanical effect of vegetation on slope stabilisation has been extensively studied (Wu et al. 1979; Mickovski et al., 2009; Bordoni et al., 2016), the plant hydrological effect, although acknowledged (Simon and Collison, 2002), has rarely been quantified and reported in the scientific literature (Stokes et al., 2014). Information on how vegetation performs hydrologically could significantly contribute to the effective and sustainable selection of plant species (Duan et al., 2016; McVicar et al., 2010) to reduce the likelihood of slope instability and the risks associated with it (Lu and Godt, 2013; Fell et al., 2005).

The hydrological effect of vegetation results from the interaction of different mechanisms occurring at the soil-plant-atmosphere continuum (Rodriguez-Iturbe and Porporato, 2004). These could be broadly divided into wetting and drying. During a rainfall event (wetting), vegetation may regulate the amount of water reaching the soil. The aerial parts (e.g. tree canopy) can intercept part of the precipitation (Llorens

and Domingo, 2007) creating an "umbrella effect" that could attenuate the amount of rainfall available to infiltrate into the soil. However, part of the rainwater will reach the soil by flowing along the stem (i.e. stemflow; Levia and Germer, 2015). Stemflow could have negative consequences upon slope stability as the water funnels around the tree base and enters the soil as a jet through the root channels (i.e. bypass flow; e.g. Liang et al., 2011). Bypass flow may induce changes in the soil stress-state (Lu and Godt, 2013) or facilitate the formation of perched water tables at depth (e.g. Simon and Collison, 2002).

The drying mechanisms are those that tend to reduce the degree of saturation of the soil after a rainfall event. Vegetation may support the drainage of water from the root zone by loosening the soil and opening preferential flow channels *via* the root system (Liang et al., 2011). However, the most acknowledged drying mechanism is the plant water uptake (e.g. Laio, 2006), which involves the withdrawal of water from the soil to satisfy plant physiological needs and transpiration into the atmosphere (i.e. evapotranspiration; e.g. Rodriguez-Iturbe and Porporato, 2004). Plant transpiration is a markedly seasonal process in temperate climates (e.g. Wever et al., 2002) and the shading effect produced by the vegetation cover can further reduce direct soil evaporation (e.g. Raz-Yaseef et al., 2010). Nonetheless, plant transpiration is meant to generate a water flow exiting the soil (Laio, 2006). This would reduce the degree of soil saturation aas well as the pore-water pressures (i.e. increasing the matric suction), potentially increasing the soil shear strength (Vanapalli et al., 1996; Gonzalez-Ollauri and Mickovski, 2017). To date, models predicting the effect of plant transpiration on the soil stress-state are severely lacking (e.g. Scanlan, 2009).

The mechanisms by which vegetation may contribute hydrologically to slope stability have been investigated before (for review see Stokes et al., 2014). A

recognised challenge, however, is their integration into slope stability analysis methods. The *unified effective stress principle* (UES; Lu and Likos, 2004) and framework (Lu and Griffiths, 2006; Lu and Godt, 2008; Lu et al., 2010), known in soil mechanics, permits the assessment of the state of stress in steep soil-mantled hillslopes under a range of water flow conditions - i.e. infiltration (wetting) or evaporation (drying). Considering these, the UES quantifies the resulting soil matric suction (Lu and Griffiths, 2006) and the associated suction stress (Lu et al., 2010); defined as the mechanical equivalent of the soil inter-particle stress. The suction stress has a negative value and affects positively (i.e. increases) the soil strength as its value becomes more negative (Lu and Godt, 2013). The intimate relationship of the suction stress to the matric suction (Lu and Likos, 2004, 2006) makes the former an ideal proxy to quantify plant-derived hydrological effects on slope stability (Gonzalez-Ollauri and Mickovski, 2017). Vegetation affects the water flow conditions through the different mechanisms discussed above (i.e. rainfall interception, stemflow, water uptake) and, hence, the soil matric suction. However, this effect has not been tested before on soils under woody vegetation using field-derived information and the UES. The UES was conceived for soil only, while the plant roots form a composite material with the soil (Thorne, 1990). This material is likely to behave hydro-mechanically differently from a fallow soil (Gonzalez-Ollauri and Mickovski, 2017) because the root systems will alter, among others, the pore size and distribution (Scanlan, 2009), the water retention dynamics (Carminati et al., 2010; Scholl et al., 2014) and the permeability of the soil (Vergani and Graf, 2015).

The aim of this study was to establish a reproducible novel framework for the evaluation of the hydrological effect of vegetation against rainfall-induced landslides. To achieve this, the following three objectives were set:

(i) To quantify *in situ* the hydrological mechanisms by which woody vegetation (i.e. *Salix* sp.) may impact the stability of a small-scale, landslide-prone, temperate humid hillslope under wetting and drying conditions.

(ii) To propose a new simplified approach to predict the plant-derived matric suction under drying conditions.

(iii) To evaluate the suitability of the unified effective stress principle and framework for quantification of the hydrological effect of vegetation against rainfall-induced landslides.

2. Study site and plant individuals

The study site is located adjacent to Catterline Bay, Aberdeenshire, UK (WGS84 Long: -2.21 Lat: 56.90; Fig. 1a), within the temperate humid climate zone (Cgc: subpolar oceanic climate; Köppen, 1884). The mean annual temperature at the site is 8.9ºC and the mean annual rainfall is 565.13 mm (2011-2014; Gonzalez-Ollauri and Mickovski, 2016). The precipitation at the site is characterised by frequent, low-intensity rainfall events (Gonzalez-Ollauri and Mickovski, 2016). Well-drained (saturated hydraulic conductivity (K_s): 5.82×10^{-05} m s^{-1}), shallow (ca. 600 mm), sloped (25-50º), and landslide-prone silty sands (sand: 79.82%; silt: 5.85 %; clay: 3.08%) overlie conglomerate rock. The topsoil at the site (0-400 mm below ground level, b.g.l.) has a mean dry bulk density of 0.86 g cm^{-3}, a drained apparent cohesion of 33.4 kPa, a mean angle of internal friction of 22º and a mean organic matter content of 5.57 %.

Two adjacent 10 m x 20 m hillslope transects with similar slope gradient (mean slope gradient: 25.6°; Figs. 1b, c) were available for studying the hydrological

effect of woody vegetation against rainfall-induced landslides. These comprised (i) a stable, willow-vegetated transect with a dense mixture of two different species of 10 year-old willow (i.e. *Salix viminalis* L. and *Salix caprea* L.) and (ii) a poorly or non-vegetated (fallow) transect that failed during the last reported instability event in the winter of 2013. Five willow individuals (two *Salix caprea* and three *Salix viminalis*) representative of the tree stand present in our study site (Fig.1) were selected for study from the willow-vegetated transect (Table 1).

Figure 1. (a) Study site location and monitoring area (yellow frame) (b) Monitoring points layout in the vegetated (X) and fallow (O) slope transect. LT: lower toe; UT: upper toe; LC: lower crest; UC: upper crest (c) Detailed view of the two monitored transects. Source aerial image: GetMapping, 2014.

Table 1. Tree metrics for the different willow individuals selected for study. *H*: tree height; *DBH*: diameter at breast height; *Ac*: canopy-crown area; *LAI*: leaf area index; *Ma*: mean aboveground biomass estimated from allometric equations for *S. viminalis* (Nordh and Verwijst, 2004) and *S. caprea* (Muukkonen and Makipaa, 2006) using *H* and *DBH* as inputs.* Individuals on which rainfall interception was studied.

Species	Individual	*H* (m)	*DBH* (m)	*Ac* (m^2)	*LAI*	*Ma* (g m^{-2})
S. viminalis	SV I*	2.84	0.44	6.54	3.26	354.68
S.viminalis	SV II*	3.65	0.39	4.24	2.67	-
S.viminalis	SV III	13.04	0.37	13.14	1.56	-
S. caprea	SC I*	4.93	0.20	13.05	3.63	2373.18
S. caprea	SC II	4.52	0.11	8.77	4.46	-

3. Methods

3.1. Quantification of the hydrological mechanisms of willow affecting slope stability under wetting and drying conditions

3.1.1. Wetting conditions

Stemflow volume was measured for the five selected willow individuals (Table 1) during the growing (July – October, 2014) and dormant seasons (November 2014 –

February 2015), respectively. For this, PVC stemflow gutters (Fig. 2a) were installed at breast height, spiralling around each tree stem and discharging into 25 L plastic containers. The stemflow volume (m^3) was scaled with the canopy-crown area (*Ac*; m^2; Table 1) and regressed against the gross rainfall (P_g; Deguchi et al., 2006) in the statistical software R v.3.2.1 (R Core Team, 2015). The magnitude of gross rainfall (P_g) was averaged from the volumes collected in 5 exposed rain gauges distributed randomly over the study site and consisting of 75 mm diameter plastic funnels attached to 2000 ml PVC bottles (Fig. 2a).

Figure 2. a) Field setup for the quantification of hydrological mechanisms of willow affecting slope stability under wetting - i.e. throughfall and stemflow b) Field setup for the quantification of hydrological mechanisms of willow affecting slope stability under drying - i.e. evapotranspiration (ETP) or plant-water uptake.

The rainfall interception could only be quantified on three individuals (i.e. two *S. viminalis* and one *S. caprea*; Table 1) with clearly delineated canopies separated from the entwined canopies in the stand. The interception was quantified during the growing (July – October, 2014) and dormant season (November 2014 – February 2015), respectively, by collecting the rainfall passing through the canopy (i.e. throughfall; Fig. 2a) into three different rain gauges placed below the canopy and at different distances from the stem for each studied individual (Table 1). The average of the water volumes collected by the undercanopy rain gauges was compared against the volume of gross rainfall (P_g). Linear regression models were fitted between the registered throughfall and gross rainfall volumes in R v.3.2.1 (i.e. revised Gash model; van Dijk and Bruijnzeel, 2001; Deguchi et al., 2006). The canopy storage capacity was appraised from the fitted regression lines (Leyton et al., 1967). The

224 rainfall interception loss was estimated to be the difference between the gross rainfall
225 and throughfall.
226 3.1.2. Drying conditions
227 The plant water uptake from the soil was quantified as soil matric suction (u_a-
228 u_w; kPa; u_a: pore-air pressure u_w: pore-water pressure; Fig. 2b; e.g. Persson, 1995) and
229 soil volumetric moisture content (θ_v) differences between the vegetated and the fallow
230 slope transect. Daily measurements of u_a-u_w and θ_v were taken with a field
231 tensiometer (Irrometer®; Fig. 2b) and a moisture profile probe (Delta-T®),
232 respectively, during the period of maximum atmospheric water demand (7th July- 18th
233 August, 2014). u_a-u_w and θ_v measurements were collected from within the soil-root
234 zone (0 - 400 mm b.g.l.; Tardio et al., 2016) at four different slope points (i.e. LT:
235 lower toe; UT: upper toe; LC: lower crest; UC: upper crest), spaced every 2 m over
236 each slope transect (Fig. 1b). The matric suction readings were collected at a single
237 soil depth (350 mm b.g.l.) at the four slope points, while the moisture readings were
238 collected at 300 and 400 mm b.g.l. at the four slope points.
239
240
241 3.2. Prediction of plant-derived matric suction under drying conditions
242 3.2.1. Approach
243 To predict the plant-derived u_a-u_w under drying conditions (Eq.1; Table 2), we
244 modified an existing closed-form equation designed to predict u_a-u_w under variable
245 steady-state water flow situations (i.e. negative sign flow: infiltration; positive sign
246 flow: evaporation) in isotropic soil materials (Eq. 2; Table 2; Lu and Griffiths, 2006;
247 for numerical derivation see Lu and Godt, 2013). Eq.2 (Table 2) is derived from the
248 integration of Darcy's law over time and space using the soil water characteristic

curve (SWCC) and the hydraulic conductivity function (HCF). We modified the original equation by: (a) replacing *Ks* by the unsaturated hydraulic conductivity ($K(\theta)$; Eq.6; Table 2), or HCF, because the soil will de-saturate as it drains or dries and because the plant water uptake will be negligible in waterlogged soils (Rodriguez-Iturbe and Porporato, 2004); and (b) introducing the canopy-crown area (Ac; m^2; Table 1) as a scaling parameter, because the entire plant crown may contribute to soil suction through plant water uptake if a top-down uptake approach is adopted (Shukla, 2014). Eq.1 (Table 2) assumes steady plant transpiration rates within the whole root zone (i.e. 0-400 m b.g.l)

3.2.2. Parameterisation

To implement Eq.1 (Table 2), knowledge of the potential daily plant transpiration rate (E_{tp}; m d^{-1} m^{-2}; Eq.3; Table 2) and the soil hydro-mechanical parameters (α: inverse of air-entry pressure, kPa^{-1}; n: pore-size distribution parameter, unitless) is needed.

To estimate E_{tp} (Eq.3; Table 2), the potential daily evapotranspiration rate (E_u; m d^{-1} m^{-2}) was calculated using the Priestly and Taylor (1972) method. For this, we employed meteorological records (i.e. daily air temperature, atmospheric pressure, and sunshine duration) retrieved from an *in situ* weather station (voor de Porte, 2011). The input variables to estimate E_u (i.e. daily solar radiation, psychrometric constant, and slope of the saturated vapor pressure at mean air temperature) were calculated as specified in Allen et al. (1998). The extension suggested by Savabi and Williams (1995) was adopted to account for different vegetation covers in terms of the leaf area index (LAI; Eq.4; Table 2) and to obtain E_{tp} from E_u (Eq.3; Table 2).

Table 2. List of equations used in this study.

Definition	Equation	Nº	Parameters	Units	Equation source
Vegetated soil matric suction under drying conditions	$u_a - u_w = Ac[\frac{-1}{\alpha}\ln\left(\left(1+\frac{E_{tp}}{K(\theta i)}\right)e^{-\gamma w \alpha z} - \frac{E_{tp}}{K(\theta i)}\right)]$	Eq.1	u_a-u_w: matric suction	kPa	This study
			Ac: canopy-crown area	m^2	
			α: inverse air-entry pressure	kPa^{-1}	
			E_{tp}: potential plant transpiration rate	m s^{-1} m^{-2}	
			$K(\theta_i)$: unsaturated hydraulic conductivity	m s^{-1}	
			θ_i: soil volumetric moisture content	/1	
			γ_w: unit weight of water	kPa m^{-1}	
			z: vertical coordinate, upward positive –i.e.soil depth from lower soil boundary (e.g. water table)	m	
Soil matric suction	$u_a - u_w = \frac{-1}{\alpha}\ln\left(\left(1+\frac{q}{Ks}\right)e^{-\gamma w \alpha z} - \frac{q}{Ks}\right)$	Eq.2	q: water flow (infiltration: negative sign; evapotranspiration: positive sign)	m s^{-1}	Lu and Griffiths (2006)
			Ks: saturated hydraulic conductivity	m s^{-1}	
Plant transpiration	$E_{tp} = \left(1 - \frac{E_{sp}}{E_u}\right)E_u$	Eq.3	E_{sp}: potential direct soil evaporation rate	m s^{-1} m^{-2}	Savabi and Williams (1995)
			E_u: potential evapotranspiration rate	m s^{-1} m^{-2}	
Direct soil evaporation	$Esp = Eue^{-0.4LAI}$	Eq.4	LAI: leaf area index	Unitless	Savabi and Williams (1995)
Soil water characteristic curve[c]	$\theta i = \theta r + (\theta s - \theta r)(\frac{1}{(1+(\alpha(u_a - u_w))^n)^{1-\frac{1}{n}}}$	Eq.5	θ_r: residual soil volumetric moisture content	/1	Van Genuchten (1980)
			θ_r: saturated soil volumetric moisture content	/1	
			n: pore size distribution parameter	Unitless	
Hydraulic conductivity function	$K(\theta i) = Ks(\frac{\theta i}{\theta s})^n$	Eq.6			Brooks and Corey (1964)
Suction stress function	$\sigma^s = -\frac{u_a - u_w}{(1+\alpha(u_a - u_w)^n)^{\frac{n-1}{n}}}$	Eq.7	σ^s: suction stress	kPa	Lu et al. (2010)
Soil shear strength (unified effective stress principle)	$\tau = c' + (\sigma - u_a - \sigma^s)tan\phi'$	Eq.8	τ: soil shear strength	kPa	Lu and Likos (2004)
			c': soil effective cohesion	kPa	
			σ: normal stress	kPa	
			u_a: pore-air pressure	kPa	
			ϕ': soil inter-particle angle of internal friction	Degrees	
Factor of Safety	$FoS = \frac{c' + (\sigma(z) - \sigma^s(z))tan\phi'}{\sigma(z)sin\beta cos\beta}$	Eq.9	FoS: factor of safety	/1	Lu and Godt (2008)
			β: slope gradient or angle	Degrees	
Normal stress	$\sigma(z) = (\gamma s(Hwt - z) + Wv)cos^2\beta$	Eq.10	σ(z): normal stress with soil depth	kPa	This study
			γ_s: soil moist unit weight	kPa m^{-1}	
			H_{wt}: water table (lower soil boundary) height	m	
			W_v: vegetation surcharge	N m^{-2}	
Bypass flow rate	$q_{by} = AcSt/t_r$	Eq.11	q_{bv}: bypass flow rate	m s^{-1}	This study
			St: stemflow volume per unit area of tree-crown	m^3 m^{-2}	
			t_r: rainfall duration	s	
Evaporative soil depth	$d_x = 0.09 - 0.0077Cl + 0.000006Sa^2$	Eq.12	d_x: maximum evaporative soil depth	m	Savabi and Williams (1995)
			Cl: percentage of clay in soil	%	
			Sa: percentage of sand in soil	%	

The soil hydro-mechanical parameters (α and n) under vegetated and fallow soil conditions, respectively, were retrieved by fitting the soil water characteristic curve (SWCC; Eq.5; Table 2; van Genuchten, 1980) for the drying path (Lu and Likos, 2004) in R v.3.2.1. To fit the SWCC, we examined the relationship between the coupled measurements of matric suction (u_a-u_w; kPa) and soil volumetric moisture content (θ_v; %) collected *in situ* over time (see 3.1.2) (e.g. Lu and Godt, 2013). Then, Eq.5 (Table 2) was fitted iteratively to the observed data points by assigning values to α and n in Eq.5 until the maximum goodness of fit (R^2) was achieved. Once the soil hydro-mechanical parameters were estimated, HCF (Eq.6; Table 2; Brooks and Corey, 1964) could be implemented in Eq.1 (Table 2) before proceeding with the plant-derived u_a-u_w predictions.

The predictions of u_a-u_w under vegetated soil were carried out using Eq.1 (Table 2) for the same days on which *in situ* u_a-u_w records were taken at the four different slope positions (see 3.1.2). For the u_a-u_w predictions, the soil moisture was assumed to be constant and at field capacity (i.e. θ_v=0.23), while the soil depth (z) was fixed at 350 mm b.g.l. The mean *Ac* among the assessed willow individuals (Table 1) was employed for the lower toe (LT), upper toe (UT) and lower crest (LC) positions. For the upper crest (UC), the canopy area of the individual adjacent to the tensiometer was used (i.e. Ac = 3.74 m^2).

3.3. Evaluation of willow hydrological effect on slope stability using the unified effective stress principle

3.3.1. Approach

Figure 3. Conceptual model for evaluating the hydrological effect of vegetation on slope stability(after Gonzalez-Ollauri and Mickovski, 2014). The forcing functions are portrayed by thick arrows and the system state variables by boxes.

We employed an existing conceptual model to evaluate the hydrological effect of willow on slope stability (Gonzalez-Ollauri and Mickovski, 2014; Fig. 3). This model considers the hydrological mechanisms quantified at the soil-plant-atmosphere interface (i.e. rainfall interception, stemflow, and plant water uptake; see 3.1) as driving functions that induce changes on the system state variables - the soil matric suction (Eq. 1 and Eq. 2; Table 2) and degree of saturation (intrinsically related to SWCC; Eq.5; Table 2). On the basis of the soil hydro-mechanical parameters (i.e. α and n; see 3.2.2), the model defines the stress-state in the soil and, ultimately, the slope stability (Figs. 3 and 4). The stress-state in the soil is depicted by the suction stress (σ^s; Eq.7; Table 2; Lu et al., 2010) featured in Coulomb's law (e.g. Head and Epps, 2011) for the estimation of the soil shear resistance (τ; Eq.8; Table 2) under variable soil saturation conditions (i.e. *unified effective stress principle*; UES; Lu and Likos, 2004). The slope stability was evaluated with the infinite slope limit equilibrium method (LEM; e.g. Craig, 2004). This estimates a factor of safety (i.e. FoS = resisting forces/driving forces; Eq.9; Table 2; Lu and Godt, 2008) and includes the UES within the resisting forces (Eq.8; Table 2). The driving forces are depicted by the normal stress ($\sigma(z)$; Eq. 10; Table 2), which includes the vegetation surcharge (W_v; Table 2), and the slope gradient (β). Herein, W_v was derived from the vegetation aboveground biomass (*Ma*; Table 1).

3.3.2 Approach testing: case scenarios and further assumptions

We tested the approach described in 3.3.1 (Fig. 3) using four discrete meteorological events (i.e. two events under wetting and drying conditions, respectively) for vegetated and fallow soil covers, and under limit equilibrium conditions (aimed at stressing the hydrological effect of vegetation under critical slope stability conditions; Lu and Godt, 2013). In all of the scenarios, the slope inclination (β) was taken as 45º, the angle of internal friction as 22º, and the soil at saturation (c=0 kPa), mimicking the onset of a rainfall-induced landslide.

a) Wetting conditions

Two rainfall episodes of different intensity were considered: (S1) the maximum rainfall event registered during the monitoring period - i.e. 15.6 mm of cumulative rainfall during 10 h; and (S2) the maximum recorded precipitation event at the study site which, presumably, triggered multiple shallow landslide events - i.e. 42.2 mm of cumulative rainfall during 10 h.

The throughfall and stemflow derived from each rainfall event were evaluated under growing and dormant states, using the regression models obtained for each mechanism and season (see 3.1.1). Both mechanisms were treated differently in terms of the infiltration process they triggered (Fig. 4). Throughfall water was assumed to infiltrate the soil as a piston flow once ponding formed on the ground surface (i.e. Green & Ampt model; Mein and Larson, 1973; see Gonzalez-Ollauri and Mickovski, 2014). The piston flow was assumed to saturate the soil (i.e. u_a-u_w = 0 kPa) as the wetting front travelled down the soil profile (Neitsch et al., 2011). The same infiltration process was considered for the fallow soil (Fig. 4). The stemflow water, however, was assumed to bypass the soil-root zone (Liang et al. 2011) as a jet flow without considering the soil anisotropy produced by the root system. Thus, stemflow

73 water would result in a water flow that infiltrates the root zone at a steady rate (q_{by};
74 Eq.11; Table 2), and produces changes in the soil stress-state as indicated in Fig.4.
75 Eq.11 (Table 2) assumed that the entire tree-crown contributed to the stemflow. The
76 formation of perched water tables in depth was neglected, and hydrostatic conditions
77 (i.e. q=0 m s^{-1}) were assumed to be below the wetting front.
78

Figure 4. Workflow diagram for the evaluation of the soil stress-state and corresponding slope stability.

79
80 b) Drying conditions
81 Two different evapotranspiration events were considered. These corresponded
82 to the days of maximum and minimum atmospheric demand registered during the
83 monitoring period (i.e. July, 7^{th} – August, 18^{th}, 2014). The soil moisture content was
84 assumed to be constant throughout the soil profile and at field capacity (i.e. θ_v=0.23).
85 For the vegetated soil, the soil stress-state was evaluated using Eq.1 (Table 2;
86 Fig. 4) assuming that the whole root system (0-400 mm b.g.l) contributed to E_{tp} (i.e.
87 steady plant transpiration rate). Hydrostatic conditions were considered to be?? below
88 the root zone (i.e. E_{tp}= 0 m s^{-1}).
89 For fallow soil, the soil stress-state was evaluated using Eq.1 (Table 2; Fig. 4),
90 with *Ac* equal to 1 m^2, and the potential soil evaporation (E_{sp}; Eq.4; Table 2) was
91 considered to be the driving function. The evaporative soil depth (d_x) was estimated to
92 be a function of the soil particle size distribution (Eq.12; Table 2; Savabi and
93 Williams, 1995). Hydrostatic conditions were assumed to be?? below d_x.
94
95 3.4. Statistical analysis

96 The statistical differences between the fitted regression models for the
97 throughfall and stemflow were examined by estimating the t-statistic at the 95% and
98 99% confidence levels (Paternoster, 1998).
99 The statistical differences between the vegetated and fallow transects, and
100 among the slope transect positions (i.e. LT, UT, LC, UC), in terms of u_a-u_w and θ_v
101 were evaluated with Kruskal-Wallis (χ^2) tests at the 95% and 99% confidence levels
102 on the basis of the degrees of freedom (df) and after pertinent statistical distribution
103 testing. When statistically significant differences were found, the differences within
104 the groups were assessed with Wilcoxon tests (W). The θ_v differences between the
105 two evaluated soil depths (i.e. 300 and 400 mm b.g.l) were assessed in the same
106 manner. The slope stability (FoS) differences between the considered treatments (i.e.
107 vegetated vs. fallow and wetting vs. drying) were evaluated using Kruskal-Wallis and
108 Wilcoxon tests.
109 The statistical differences between the observations and predictions (i.e.
110 goodness of fit) for the plant-derived soil matric suction under drying conditions were
111 analysed with F-tests (i.e. variance test). Additionally, ARIMA (autoregressive
112 integrated moving average) models were fitted to each time series (i.e. observed and
113 predicted) after carrying out autocorrelation tests (Cowpertwait and Metcalfe, 2009).
114 The models were then compared on the basis of AIC (Akaike information criterion).
115
116
117 # 4. Results
118
119 ## 4.1. Quantification of the hydrological mechanisms of willow affecting slope
120 stability under wetting and drying conditions
121 ### 4.1.1. Wetting conditions

The throughfall and stemflow (Table 3 and Fig. 5) showed a linear correlation with the gross rainfall (P_g) in all cases. *S. viminalis* showed a positive rainfall interception capacity for the growing (S1: 26.73%; S2:22.03%) and dormant (S1:8.91%; S2:2.25%) seasons under both rainfall scenarios (Table 3). *S. caprea,* however, only presented a positive rainfall interception capacity for the dormant season under both rainfall scenarios (S1:16.73%; S2:16.27%; Table 3). The overall canopy storage capacity was 0.72 and 0.41 for *S. viminalis* and *S.caprea*, respectively. There were no statistical differences in throughfall between the two willow species for the global fitted models (i.e. using all monitoring points; $t=0.84$, $df=48$, $p>0.05$). However, significant differences between the growing and dormant seasons in terms of throughfall were observed for *S. caprea* ($t=2.61$, $df=3$, $p<0.05$).

Figure 5. Observed (points) and regressed (lines) hydrological data with respect to the gross rainfall during the growing and dormant seasons for (a) interception, *Salix viminalis* (b) interception, *Salix caprea* (c) stemflow, *Salix viminalis* (d) stemflow, *Salix caprea*. Global fit: linear regression for the entire data set. Data points are derived from the cumulative rainfall belonging to discrete rainfall events (i.e. data points closer to origin; $P_g < 20$ mm) and multiple rainfall events combined (i.e. data points farther from the origin; $P_g > 20$ mm).

The water volume concentrated around the stem was higher for *S. caprea*, reaching volumes beyond 45 L (10.78% of rainfall) under the heavy rainfall scenario (S2) for both seasons (Table 3). The stemflow showed significant differences between the two willow species for the fitted global regressions ($t=2.95$, $df=48$, $p<0.01$). Seasonal differences were also observed for the two willow species (*S. viminalis*: $t=6.86$, $df=6$, $p<0.01$; *S. caprea*: $t=2.07$, $df=11$, $p<0.05$). The bypass flow rates derived from the stemflow under the two considered rainfall scenarios (S1 and S2) are shown in Table 3.

Table 3. Throughfall (Th) and stemflow (St) linear relationships with gross rainfall (P_g), and predicted outcomes for rainfall interception (i_x), stemflow volume (St_x) and bypass flow rate (q_{by-x}) under the two rainfall scenarios considered - i.e. S1: 15.6 mm during 10 h ; S2: 42.2 mm during 10 h. R^2: regression lines goodness of fit. Global fit: linear regression fitted with every monitoring data.

			Fitted		Predicted		Fitted		Predicted			
Species	Individual	Season	Throughfall	R^2	i_{S1} (mm)	i_{S2} (mm)	Stemflow	R^2	St_{S1} (L)	St_{S2} (L)	q_{by-S1} (m s^{-1})	q_{by-S2} (m s^{-1})
S. viminalis	SV I		$Th=1.42P_g-9.09$	0.89			$St=0.01P_g+0.03$	0.72				
S. viminalis	SV II		$Th=0.61P_g-1.21$	0.93			$St=0.06P_g-0.10$	0.82				
S. viminalis	SV III		-	-			$St=0.05P_g-0.12$	0.89				
S. viminalis		Growing	$Th=0.81P_g-1.21$	0.68	4.17	8.81	$St=0.05P_g-0.14$	0.66	5.10	14.82	-1.23e-07	-3.79e-07
S. viminalis	Combined	Dormant	$Th=1.02P_g-1.7$	0.60	1.39	0.90	$St=0.015P_g+0.03$	0.97	2.10	5.02	-5.08e-08	-1.27e-07
S. viminalis		Global	$Th=1.02P_g-5.14$	0.74			$St=0.03P_g+0.23$	0.49				
S. caprea	SC I		$Th=0.91P_g+4.86$	0.82			$St=0.05P_g-0.13$	0.67				
S.caprea	SC II		-	-			$St=0.06P_g-0.04$	0.49				
S. caprea		Growing	$Th=1.50P_g-6.77$	0.83	-1.03	-13.23	$St=0.053P_g-0.07$	0.58	8.25	45.50	-7.77e-07	-3.37e-06
S.caprea	Combined	Dormant	$Th=0.84P_g-0.11$	0.86	2.61	6.51	$St=0.14P_g-1.05$	0.48	12.37	49.64	-4.66e-07	-1.38e-06
S. caprea		Global	$Th=0.91P_g+4.86$	0.82			$St=0.05P_g-0.10$	0.61				

158

159 4.1.2. Drying conditions

160 When compared with the fallow slope transect, the vegetated transect showed
161 significantly lower (χ^2=53.94, df=1, p<0.01) soil moisture and (θ_v; Fig. 6a-d) and
162 significantly higher matric suction (u_a-u_w; Fig. 7a-d) (χ^2=52.07, df=1, p<0.01).

163 The soil moisture increased significantly with soil depth (W=6027, p<0.01;
164 Fig. 6a-d), and was, on average, 12.84 % higher in the fallow transect when compared
165 with the vegetated one. The fallow transect showed significant differences in terms of
166 θ_v between the slope positions (χ^2=28.35, df=3, p<0.01) with the UC shown to be the
167 driest (Fig. 1b; W=1284, p<0.01) position on the slope. The vegetated transect did not
168 show significant differences in soil moisture between the slope positions (χ^2=5.78,
169 df=3, p=0.12).

170

171 Figure 6. Measured (points and crosses) and interpolated (lines) volumetric moisture content (θ_v) time series for the fallow slope transect and willow-vegetated slope transect at two soil depths (300 mm and 400 mm b.g.l) and at four different slope locations (a) lower toe (LT) (b) upper toe (UT) (c) lower crest (LC) (d) upper crest (UC). Top and right-hand side axes: daily rainfall (mm d^{-1}) time series.

172

173 In the willow-vegetated transect, where the suction was kept above 10 kPa
174 over the monitoring period at all slope positions (Fig. 1b), u_a-u_w (Fig. 7a-d) reached
175 peaks of ca. 60 kPa. In the fallow transect, u_a-u_w was well below 20 kPa for most of
176 the monitoring time and at all 4 slope positions, where saturation levels of suction (i.e.
177 0 kPa) were reached during the monitoring period (Fig. 7a-d). For both treatments, u_a-
178 u_w showed significant differences between slope positions (Willow: χ^2=27.89, df=3,
179 p<0.01; Fallow: χ^2=15.04, df=3, p<0.01). UC (Fig. 1b) showed the lowest suction
180 levels in the vegetated transect (W=342, p<0.01).

181

182 Figure 7. Measured (points and crosses), interpolated (dotted lines) and predicted (solid and dashed lines) matric suction (u_a-u_w) time series for fallow slope transect and willow-vegetated transect at the four different slope locations (a) lower toe (LT) (b) upper toe (UT) (c) lower crest (LC) (d) upper crest (UC). Model 1: Predictions obtained using Eq.2; Model 2: Predictions obtained using Eq.1. Top and right-hand side axes: daily rainfall (mm d^{-1}) time series

183

184

185 4.2. Prediction of plant-derived matric suction under drying conditions

186 4.2.1. Approach parameters

187 The parameter values using Eq.1 (Table 2) and predicting plant-induced u_a-

188 u_w under drying conditions are shown in Table 4.

189 A statistically significant relationship between u_a-u_w and θ_v (i.e. SWCC; Table

190 4; Fig. 8a) was found at all slope positions for the fallow transect after fitting Eq.5

191 (Table 2) using the monitoring data (Figs. 6 and 7). Only the SWCC fitted for LC

192 (Fig. 1b) differed from the curves fitted for the other three slope positions (Fig. 8a). A

193 statistically significant relationship between u_a-u_w and θ_v was not encountered for the

194 vegetated slope transect (Fig. 8b). Consequently, the hydro-mechanical parameters for

195 the willow-vegetated soil could not be obtained. The mean α (Table 2) from the LT,

196 UT, and UC slope positions (Table 4) was used in Eq.1 (Table 2). To evaluate the

197 soil stress-state (Eq. 7; Table 2) under vegetation cover and drying conditions, the

198 value of n (Table 2) was assigned arbitrarily (Table 4) in agreement with published

199 values for vegetated soil (Carminati et al., 2010).

200 Figure 8. Soil water characteristic curves (SWCCs) for (a) fallow soil transect (b) willow-vegetated transect obtained at: LT - lower toe; UT - upper toe; LC - lower crest; and UC - upper crest slope positions.

201

202 4.2.2. Matric suction predictions

203 The plant-derived soil matric suctions under drying conditions were

204 successfully predicted using Eq. 1 (Fig. 7). No statistical differences were detected

205 between the observations and model predictions except for the LC position (Table 4).

Table 4. Parameters value used in the implementation of Eqs. 1 and 7 (Table 1) for predicting plant-derived matric suctions, and the subsequent suction stress, under the scenarios of maximum (Max) and minimum (Min) atmospheric demand. Bottom part: goodness of fit (i.e. F-statistic and AIC) between predicted plant-derived matric suction time series and monitored field values. Slope positions: LT: lower toe; UT: Upper toe; LC: lower crest; UC: upper crest.

		Fallow soil				Vegetated soil			
						Salix viminalis		*Salix caprea*	
Parameter	Definition	Max		Min		Max	Min	Max	Min
E_u	Potential daily evapotranspiration rate; m d^{-1} m^{-2}	-		-		6.28e-08	1.96e-08	6.38e-08	1.99e-08
E_{tp}	Potential daily plant transpiration rate; m d^{-1} m^{-2}	-		-		3.97e-08	1.23e-08	5.12e-08	1.59e-08
E_{sp}	Potential daily soil evaporation rate; m d^{-1} m^{-2}	1.42e-11		4.42e-12		1.83e-11	5.71e-12	1.00e-11	3.13e-12
d_x	Evaporative soil depth; m	0.13				-			
$K(\theta)$	Unsaturated hydraulic conductivity; m s^{-1}	2.31e-08				2.31e-08			
	Slope position	LT	UT	LC	UC	LT	UT	LC	UC
α	Inverse air-entry pressure; kPa^{-1}	0.06	0.05	0.2	0.06	0.05			
n	Pore-size distribution parameter; unitless	6.00	5.00	2.23	5.00	2.00			
R^2	Coefficient of determination for SWCC	0.90	0.74	0.70	0.73	-			
F-statistic (df=15)	Variance test statistic from u_a-u_w model validation					0.91	2.62	4.58	0.92
p-value	Significance level from variance test					0.86	0.07	< 0.01	0.87
AIC	Akaike information criterion from ARIMA					115.18	132.21	141.07	90.56

All of the studied time series were stationary on the basis of the autocorrelation tests. The ARIMA models fitted for the LT and UC positions presented higher goodness of fit (Table 4) than ???????.

4.3. Evaluation of willow hydrological effect on slope stability using the unified effective stress principle

The suction stress profiles (Figs. 9a-d) predicted with Eq.7 (Table 2) presented consistent differences between wetting (Figs. 9a-c) and drying (Fig. 9d) conditions as well as between fallow and vegetated soil. These differences were mainly attributed to the differences in the hydro-mechanical parameters between the fallow and willow-vegetated soil (Table 4) and the infiltration process under consideration (Fig. 4). While the infiltration as a piston flow tended to dramatically reduce the suction stress (Figs. 9a-c), the stemflow-derived bypass infiltration did not significantly change the soil stress-state conditions with respect to hydrostatic state (shown in Fig. 9d as grey dashed line).

Figure 9. (a) Suction stress (σ^s) profiles produced by the hydrological mechanisms evaluated under wetting conditions (i.e. throughfall and stemflow) for *S.viminalis* and *S.caprea* for the dormant season under the two wetting scenarios (S1 and S2) (b) Suction stress (σ^s) profiles produced by the hydrological mechanisms evaluated under wetting conditions (i.e. throughfall and stemflow) for *S.viminalis* and *S.caprea* for the growing season under the two wetting scenarios (S1 and S2) (c) Suction stress (σ^s) profiles for fallow soil under the two wetting scenarios (S1 and S2) (d) Suction stress (σ^s) profiles produced by the hydrological mechanism evaluated under drying conditions for *S.viminalis*, *S.caprea* (i.e. plant transpiration; Etp) and fallow soil (i.e. direct soil evaporation; Esp) under the two atmospheric demand scenarios (Max. Etp and Min. Etp); Dotted line: σ^s profile under drying conditions assuming non-composite material; Dashed line: hydrostatic σ^s profile (e) Factor of Safety (FoS) profiles under vegetated soil for the selected wetting and drying events (f) Factor of Safety (FoS) profiles under fallow soil for the selected wetting and drying events. FoS>1.0 denotes a stable slope in engineering terms (Craig, 2004).

The FoS profiles (Figs. 9e-f) predicted with Eq.9 (Table 2) showed agreement with the suction stress profiles (Figs. 9a-d). Drastic reductions in suction stress resulted in instability zones (i.e. FoS < 1) in the FoS profiles (Figs. 9e-f). The increase

237 in suction stress under drying conditions (Fig. 9d) appeared to shift the FoS profiles
238 towards values denoting stability (i.e. FoS > 1; Figs. 9e-f) when compared with the
239 wetting conditions. As a result of this, the FoS distribution showed significant
240 differences between the wetting and drying conditions (χ^2=82.18, df=1, p<0.01), as
241 well as between the fallow and vegetated soil (χ^2=11.75, df=1, p<0.01). FoS
242 differences between the willow species were not detected under wetting or drying
243 conditions. However, the FoS derived from the throughfall effect (Fig. 9e) showed
244 significant differences under the heavy rain scenario (S2; χ^2=7.49, df=1, p<0.01).
245 Under drying conditions, significant differences were observed between the
246 maximum and minimum E_{tp} scenarios (χ^2=19.13, df=1, p<0.01).
247 Values of FoS below unity were predicted for soil depths of 400 mm b.g.l and
248 deeper (Figs. 9e-f). This outcome was due to the assumptions of soil strength (i.e. c=0
249 kPa) and a very steep slope (i.e. β=45°) which highlighted the hydrological effect of
250 *Salix* sp. under critical stability conditions. Under this setting (unrealistic for our
251 study site with mean soil cohesion of 33 kPa and mean slope gradient of 25°), the
252 stress generated by the weight of the soil column counteracted the shear resistance
253 provided by the angle of internal friction. The latter was not high enough to provide
254 stable slope conditions in the absence of cohesion (Lu and Godt, 2013), leading to the
255 occurrence of failure zones in the FoS profiles (Figs. 9e-f).
256
257 5. Discussion
258
259 5.1. Quantification of the hydrological mechanisms of willow affecting slope
260 stability under wetting and drying conditions
261 5.1.1. Wetting conditions:

The rainfall interception (i.e. gross rainfall minus throughfall) by *Salix viminalis* (Fig. 5a; Table 3) noticeably affected the amount of rain that eventually reached and entered the ground. This effect was observed to be seasonal (Table 3; Fig. 5a) due to foliage cover (Deguchi et al., 2006). However, under the heavy rainfall scenario (i.e.. S2; see 3.3.1), the interception capacity decreased (Table 3) as a result of the canopy saturation (van Dijk and Bruijnzeel, 2001). This suggests that under heavy precipitation events, such as the ones normally triggering landslides (Sidle and Bogaard, 2016), most of the rain will reach the ground. However, rainfall interception can still be useful in regulating the water mass balance in the soil (Llorens and Domingo, 2007), preventing the soil from reaching saturation moisture levels during prolonged periods of gentle rain (i.e. typical meteorological conditions at our study site) and, potentially improving the slope stability conditions (Lu and Godt, 2013).

The throughfall regression model for *Salix caprea* predicted more throughfall than the gross rainfall for the growing season (Table 3). This may result from dripfall (Zimmermann and Zimmermann, 2014) – the rainwater that accumulates on leaves and falls to the ground once the canopy has become saturated (van Dijk and Bruijnzeel, 2001) – which would have been significant due to the fact that the observed canopy storage capacity for *S. caprea* was rather low (see 4.1.1; Deguchi et al., 2006). Dripfall patterns are likely to be random, as the architecture of tree canopies is highly heterogeneous (e.g. Bohrer et al., 2009). As a result, a given interception rain gauge may collect larger water volumes than originally expected. This anomaly could be corrected by changing the setup approach to monitor a larger canopy area (Zimmermann and Zimmermann, 2014). In our case, however, a broader canopy area could not be taken for study due to the site operational difficulties (i.e. steep and densely vegetated slope prone to instability) and the entwined canopies in

287 the stand. Nonetheless, the method outlined here for evaluating throughfall for slopes
288 under dense vegetated zones was shown to be feasible. Future studies should focus on
289 addressing the indicated shortcomings to obtain reliable rainfall interception models
290 in these environmental contexts.

291 The stemflow results (Figs. 5c-d; Table 3) indicated that the concentration of
292 water around the stem can be substantial (Liang et al., 2011; Levia and Germer,
293 2015). Stemflow differences observed between the studied species suggest that the
294 canopy morphology (e.g. branch architecture, tree-crown spread) may also govern this
295 mechanism (Yuan et al., 2016). Stemflow water could be funnelled around the tree
296 base and enter the soil as a bypass flow (Liang et al., 2011) with potential effects on
297 the soil stress-state (Lu and Godt, 2013). Thus, careful consideration of plant aerial
298 traits may help to highlight the intra-species differences in terms of stemflow (Levia
299 and Germer, 2015). In any case, the method presented here was shown to be viable
300 for quantifying the volumes of water concentrated around the stems of woody
301 vegetation growing on slopes. Our study has also shown that the stemflow process
302 deserves more attention in order to better understand the water cycle dynamics on
303 vegetated slopes (Levia and Germer, 2015).

304

305 5.1.2. Drying conditions

306 The plant-water uptake, assessed through the measurement of θ_v (Fig. 6a-d)
307 and u_a-u_w differences between vegetated and fallow soil over time (Fig. 7a-d), was
308 evident in all cases (Persson, 1995; Ng et al., 2013). This stresses the positive
309 hydrological effect of vegetation in terms of the soil water balance regulation in a
310 slope stability context (Stokes et al., 2008). The vegetation showed a pronounced
311 effect upon the increase of u_a-u_w (Fig. 7a-d) and on the desaturation or drainage (i.e.

312 θ_v increased with soil depth; Fig. 6a-d) of the soil profile, suggesting that vegetation
313 increases slope stability (Wilkinson et al., 2002). This effect appeared to be stronger
314 at the lower toe of the slope (Fig. 7a) which may have been due to a denser vegetation
315 cover at the slope toe in the willow-vegetated transect. The denser vegetation cover
316 may have been favoured by a more gentle slope gradient at the landslide deposition
317 zone (i.e. slope toe), where soil nutrients tend to accumulate (Walker et al., 2009;
318 Gonzalez-Ollauri and Mickovski, In Press). A denser plant cover could have led to a
319 higher plant-water demand (Jia et al., 2017) which, in turn, helped tomaintain higher
320 suction (Fig. 7a) and lower moisture levels (Fig. 6a) in the soil.
321 There appeared to be an effect of climate on the soil moisture dynamics (e.g.
322 Zhang et al., 2016) in our observations as both u_a-u_w and θ_v were affected by changes
323 in precipitation patterns (Figs. 6 and 7) – soil input water from rainfall led to marked
324 decreases in u_a-u_w and increases in θ_v as rain infiltrated into the soil profile. However,
325 this observation could not be fully quantified because of the relatively short
326 monitoring period, which we acknowledge to be a limitation of our study. A temporal
327 expansion of the study would help the evaluation the hydrological effect of vegetation
328 under different seasonal conditions (e.g. winter, when atmospheric demand of water is
329 low in temperate climates), and derivation of a clearer numerical relationship between
330 rainfall, u_a-u_w, and θ_v.
331
332 5.2. Prediction of plant-derived matric suction under drying conditions
333 The plant-derived matric suction predictions (Fig. 7a-d) using Eq. 1 (Table 2) matched
334 well the monitoring (Fig. 7a-d) and fell within the range observed *in situ*. The
335 predictive capacity of our approach could be enhanced in the future by revising some
336 of the assumptions made to reduce the computational effort. For example, we

337 considered a constant $K(\theta)$ (i.e. the one corresponding to the water content at field
338 capacity; Table 4) instead of allowing it to vary with the soil moisture overtime.
339 Additionally, the same *Ac* (Table 1) was considered for three of the four monitored
340 slope positions. Finally, E_{tp} (Table 4) estimations can vary from approach to approach
341 (Li et al., 2016) and the required inputs are subject to many inaccuracies depending
342 upon the meteorological station from where they had been retrieved. The E_{tp}
343 estimation was particularly sensitive to sunlight duration, which, at our site with
344 mainly overcast days, tended to be negligible and led to low estimation of E_{tp}. All of
345 these, together with the soil moisture buffering behaviour induced by plant roots (i.e.
346 upon drying the root system tends to hold more water, while upon wetting it tends to
347 remain drier than the surrounding bulk soil; Carminati et al., (2010), could explain the
348 time lags between predictions and observations (Fig. 7a-c).

349 The original equation (Eq.2; Lu and Griffiths, 2006) predicted invariant (ca.
350 2.5 kPa) u_a-u_w time series that were well below the *in situ* observations (Fig. 7a-d)
351 because it did not incorporate the effects of vegetation. The unsuccessful
352 determination of the hydro-mechanical parameters (α and n) for vegetated soil (Fig.
353 8b; Table 4) suggests that the relationship between plant, soil and water is more
354 complex than the one between soil and water alone. This supports the idea of plant-
355 soil composite materials (Thorne, 1990) behaving hydro-mechanically differently
356 from soil alone (Scanlan, 2009; Gonzalez-Ollauri and Mickovski, 2017). The
357 determination of α and n could potentially have been obscured by either microscopic
358 or macroscopic issues. On the one hand, the release of root mucilage could have
359 altered the relationship between water content and matric potential in the root zone
360 (Read and Gregory,1997; Read et al., 2003). On the other, plant effects on the soil
361 structural properties (e.g. Bronick and Lal, 2005; Scholl et al., 2014) may have

362 modified the hydrological behaviour of the soil (Liang et al., 2011). Further
363 investigation should be carried out to confirm our observations and develop new,
364 robust models that are able to predict u_a-u_w, as well as SWCC, under the effect of
365 vegetation, instead of assigning new and different hydro-mechanical parameters to
366 vegetated soils alone (Scanlan, 2009; Carminati et al., 2010; Leung et al., 2015).
367 Moreover, an extension of the monitoring period, as indicated before, and inclusion of
368 different plant species, would potentially clarify the feasibility of the suggested
369 approach. Nonetheless, we believe that our model opens up an exciting possibility for
370 the assessment of the plant-derived hydrological effect in a slope stability context,
371 given the high relevance of u_a-u_w to the soil stress-state (Vanapalli et al., 1996; Lu and
372 Likos, 2004; Gonzalez-Ollauri and Mickovski, 2017).
373
374 5.3. Evaluation of willow hydrological effect on slope stability using the unified
375 effective stress principle
376 Overall, the unified effective stress principle (UES) was shown to be adequate
377 for capturing the hydrological effect of vegetation on slope stability (Fig. 9). Our
378 results support the hypothesis that plant-water uptake is the main hydrological
379 mechanism by which vegetation can improve slope stability (Figs. 9d and e; Stokes et
380 al., 2014). Under drying conditions, the soil strength (i.e. σ^s; Fig. 9d) improved
381 substantially with respect to the wetting (Figs. 9a-c) and hydrostatic (dashed dark grey
382 line in Fig. 9d) conditions. However, this effect is expected to be markedly seasonal
383 in temperate climates where the atmospheric water demand is expected to be
384 negligible in winter (Wever et al., 2002). The differences between the two willow
385 species upon drying (Figs. 9d and e) reflect the assumption made with regard to the
386 effect of canopy features (i.e. *Ac* and *LAI*; Table 1; Eqs.1, 3 and 4; Table 2) on the soil

387 stress-state and slope stability. A wider canopy with broader leaves (i.e. higher *LAI*;
388 Table 1) led to higher transpiration rates (Table 4; Allen et al., 1998), which increased
389 the soil strength (Fig. 9d) and slope stability (Fig. 9e). Our results (Fig. 9d) reflect the
390 differences in water flow rates upon drying (i.e. plant transpiration vs. soil
391 evaporation; Table 4) as well as the hydro-mechanical differences between plant-soil
392 composites and soil materials (Table 4). If alternative, and lower *n* values were not
393 given to vegetated soil (Table 4), the hydrological effect of willow on the soil stress-
394 state would have been negative in respect of the fallow soil upon drying (Fig. 9d)
395 which would have been contradictory to the field observations (e.g. Simon and
396 Collison, 2002). Thus, the hydro-mechanical change provoked by the presence of
397 vegetation in the soil is expected to have considerable hydrological implications for
398 slope stability (e.g. Gonzalez-Ollauri and Mickovski, 2017). The quantification of
399 these emergent plant-soil composite properties is still a major knowledge gap that
400 needs further investigation (e.g. Scanlan, 2009; Carminati et al., 2010).

401 Under wetting conditions (Figs. 9a-c), vegetation effect on slope stability was
402 minimal (Fig. 9e-f). This outcome stresses the mechanical role of vegetation (i.e. soil-
403 root reinforcement; Stokes et al., 2008; Gonzalez-Ollauri and Mickovski, 2016) under
404 critical hydrological conditions of slope stability. The FoS profiles (Fig. 9e) would
405 not have presented failure zones (i.e. FoS < 1) under wetting conditions if the
406 apparent root cohesion had been included in the analysis (Wu et al., 1979; Mickovski
407 et al., 2009; Gonzalez-Ollauri and Mickovski, 2014). Yet, the effect of plant aerial
408 features on the belowground hydrological dynamics became evident with the
409 implementation of UES. The investigation of shortcomings discussed for *Salix caprea*
410 in Section 5.1 led to the prediction of a negative hydrological effect on the soil-stress
411 state (Figs. 9a-b) with respect to the fallow soil (Fig. 9c). However, *Salix viminalis*

showed a positive ability to intercept rainfall (Table 3; Fig. 5a). This resulted in a shallower wetting front (Figs. 9a and b) with respect to the fallow soil (Fig. 9c). The latter was particularly noticeable during the growing season and under the heavy rainfall scenario (Fig. 9b). As a result, the location of the potential slope failure plane was shown to be shallower under *S. viminalis* with respect to the fallow soil (Figs. 9e-f). This effect, albeit small, could make a difference in terms of slope stability and in terms of the soil volume wasted during landslide episodes (Gonzalez-Ollauri and Mickovski, 2016).

The bypass flow (Table 2) triggered by stemflow (Table 3; Figs. 5c-d; Liang et al., 2011) did not produce soil stress-state changes (Fig. 9a-b) with respect to the hydrostatic conditions (Fig. 9d). As a result, the stemflow had a negligible effect on slope stability (Fig. 9e). Nonetheless, we stress, once again, that stemflow deserves further attention (Levia and Germer, 2015) in studies focusing on slope stability with the use of vegetation. Such studies should focus on the plant traits favouring the formation of stemflow (Yuan et al., 2016) and on the clarification of the features of the infiltration process triggered by stemflow (Liang et al., 2011).

6. Conclusions

This study provides a novel and reproducible framework that sets the basis for effective evaluation of the hydrological effect of vegetation on slope stability and to shed more light on the hydrological mechanisms involved. In light of our observations and findings, it can be concluded that:

- When compared to fallow soil, willow had a noticeable hydrological effect on the soil. This was seen in differences in the recorded time series for u_a-u_w and θ_v, revealing the potential soil desaturation effect of vegetation and its subsequent positive effect on slope stability.
- Willow throughfall and stemflow mechanisms were observed and they followed a linear relationship with the gross rainfall that changed seasonally. However, they were highly influenced by canopy heterogeneity and their effect on slope stability was minimal.
- Plant-derived matric suction under drying conditions was successfully predicted with the proposed approach within the onsite observed u_a-u_w range. This novel approach for assessment of the hydrological effect of vegetation on slope stability can be improved and further validated with longer time series and different plant species.
- The unified effective stress principle and framework (UES) was shown to be adequate for evaluating the hydrological effect of vegetation on slope stability. This approach, however, requires knowledge of the soil hydro-mechanical properties, which showed differences between plant-soil composite and fallow soil materials that need further investigation.

In this paper, we have pointed out the aspects that deserve further consideration upon using UES for the evaluation of the hydrological effect of vegetation on rainfall-induced landslides. We encourage testing the framework presented herein under different environmental settings (i.e. climate, vegetation, soil hysteretical conditions, seasons, etc.).

462 Acknowledgments

463 The authors thank to Catterline Brae Action Group (CBAG) for site access and
464 logistical support. Special thanks to Pieter voor de Porte for supplying meteorological
465 data. The help of students funded by international programmes, Leonardo Gentile and
466 Gabriel Maraslis (Science Without Borders students) is greatly acknowledged. We
467 are grateful to Elizabeth Mittell for language and style editing. We also acknowledge
468 the useful comments and suggestions from the Editors and two anonymous referees
469 that helped us to enhance this manuscript. This research project was funded by a PhD
470 scholarship awarded by the School of Engineering and Built Environment at the
471 Glasgow Caledonian University (S1340554).

472 **References**

473

474 Allen, R. Pereira, L., Raes, D., Smith, M., 1998. Crop evapotranspiration guidelines
475 for computing crop water requirements. FAO Irrigation and drainage paper No
476 56.

477 Bohrer, G., Katul, G.G., Walko, R.L., Avissar, R., 2009. Exploring the effects of microscale
478 structural heterogeneity of forest canopies using large-eddy simulations. Boundary-Layer
479 Meteorology, 132, 351-382.

480 Bordoni M., Meisina C., Vercesi A., Bischetti G.B., Chiaradia E.A., Vergani C., Chersich S.,
481 Valentino R., Bittelli M., Comolli R., Persichillo M.G., Cislaghi A., 2016. Quantifying
482 the contribution of grapevine roots to soil mechanical reinforcement in an area
483 susceptible to shallow landslides. Soil & Tillage Research, 163, 195-206.

484 Bronick, C. and Lal, R., 2005. Soil structure and management: a review. Geoderma.
485 124, 3-22.

Brooks, R. and Corey, A., 1964. Hydraulic properties of porosus media (Vol.3). Hydrology Papers-Colorado State University. Fort Collins, Colorado, US.

Carminati, A., Moradi, A.B., Vetterlein, D., Vontobel, P., Lehmann, E., Weller, U., Vogel, H. and Oswald, S.E., 2010. Dynamics of soil water content in the rhizosphere. Plant Soil, 332, 163-176

Collison, A. and Anderson, M.G., 1996. Using combined slope hydrology/stability model to identify suitable conditions for lanslide prevention by vegetation in the humid tropics. Earth Surface Processes and Landforms, 21, 737-747.

Cowpertwait, P. S. P. and Metcalfe, A. V., 2009. Introductory time series with R. Springer, Doerdrecht, The Netherlands.

Craig, R., 2004. Craig's Soil Mechanics 7th Edition. E and FN Spon. London, UK

Deguchi, A., Hattori, S., and Park, H., 2006. The influence of seasonal changes in canopy structure on interception loss: Application of the revised Gash model. Journal of Hydrology, 318, 80-102.

Duan, L., Huang, M., Zhang, L., 2016. Differences in hydrological responses for different vegetation types on steep slope on the Loess Plateau, China. Journal of Hydrology, 537, 356-366.

Gonzalez-Ollauri, A. and Mickovski, S.B., 2014. Integrated model for the hydro-mechanical effects of vegetation against shallow landslides. EQA, 13, 35-59.

Gonzalez-Ollauri, A. and Mickovski, S. B., 2016. Using the root spread information of pioneer plants to quantify their mitigation potential against shallow landslides and erosion. Ecological Engineering, 95,302-315.

Gonzalez-Ollauri, A. and Mickovski, S.B., 2017. Plant-soil reinforcement response under different soil hydrological regimes. Geoderma, 285, 141-150.

510 Gonzalez-Ollauri, A. and Mickovski, S.B., In Press. Shallow landslides as drivers for
511 slope ecosystem evolution and biophysical diversity. Landslides, DOI:
512 10.1007/s10346-017-0822-y
513 Fell, R, Ho, K.K.S., Lacasse, S., Leroi, E., 2005. A framework for landslide risk
514 assessment and management. In: Hungr, Fell, Couture and Eberhardt (eds).
515 Landslide risk management. Taylor and Francis Group, London.
516 Head, K. H. and Epps, R. J., 2011. Manual of Soil Laboratory Testing: Permeability.
517 Shear Strenght and Compressibility Tests (Vol. 2). CRC Press, Boca Raton, US.
518
519 Jia, X., Shao, M., Zhu, Y., Luo, Y., 2017. Soil moisture decline due to afforestation
520 across the Loess Plateau, China. Journal of Hydrology, 546, 113-122.
521 Köppen, W., 1884. The thermal zones of the Earth according to the duration of hot,
522 moderate amd cold periods and the impact of heat on the organic world.
523 Meteorol. Z. 1, 215-226.
524 Kramer, P. and Boyer, J.S., 1995. Water relations of plants and soils. Elsevier
525 Science, San Diego, US.
526 Laio, F., 2006. A vertically extended stochastic model of soil moisture in the root
527 zone. Water Resources Research. 43 (W02406).
528 Laio, F., D'Odorico, P., Ridolfi, L., 2006. An analytical model to relate the vertical
529 root distribution to climate and soil properties. Geophys. Res. Lett., 33, L18401.
530 Leung, A.K., Garg, A., Ng., C.W.W., 2015. Effects of plant roots on soil-water
531 retention and induced suction in vegetated soil. Engineering Geology, 193, 183-
532 197.

533 Levia, D.F. and Germer, S., 2015. A review on stemflow generation dynamics and
534 stemflow-environment interactions in forests and shrublands. Review of
535 Geopgysics, 53, 673-714.
536 Li, S., Kang, S., Zhang, L., Zhang, J., Du, T., Ding, R., 2016. Evaluation of six
537 potential evapotranspiration models for estimating crop potential and actual
538 evapotranspiration in arid regions. Journal of Hydrology, 543, 450-461.
539 Liang, W., Kosugi, K. and Mizuyama, T., 2011. Soil water dynamics around a tree
540 on a hillslope with or without rainwater supplied by stemflow. Water Resources
541 Research, 47 (W02541).
542 Llorens, P. and Domingo, F., 2007. Rainfall partitioning by vegetation under
543 Mediterranean conditions. A review of studies in Europe. Journal of Hydrology,
544 335, 37-54.
545 Lu, N. and Likos, W. J., 2004. Unsaturated Soil Mechanics. John Wiley and Sons,
546 Hoboken, US.
547 Lu, N. and Giffiths, D., 2006. Profiles of steady-state suction stress in unsaturated
548 soils. J. Geotech. Geoenviron. Eng., 130 (10), 1063-1076.
549 Lu, N., Godt, J.W., 2008. Infinite slope stability under steady unsaturated seepage
550 conditions. Water Resources Research., 44 (W11404).
551 Lu, N., and Godt, J., 2013. Hillslope Hydrology and Stability. Cambridge University
552 Press, New York, US.
553 Lu, N., Godt, J. and Wu, D., 2010. A closed-form equation for effective stress in
554 unsaturated soil. Water Resources Research, 46 (5), 1-14.
555 McVicar, T.R., van Niel, T.G., Li. L.T., Wen, Z.M., Yang. Q.K., Li, R., Jiao, F.,
556 2010. Parsimoniously modelling perennial vegetation suitability and identifying
557 priority areas to support China's re-vegetation program in the Loesss Plateau:

558 Matching model complexity to data availability. Forest Ecology and
559 Management, 259(7), 1277-1290.
560 Mein, R. and Larson, C., 1973. Modeling infiltration during steady rain. Water
561 Resources Research, 9 (2), 384-394.
562 Mickovski, S., Hallet, P., Bransby, M., Davis, M., Sonnenberg, R., and Bengough, A.,
563 2009. Mechanical Reinforcement of Soil by Willow Roots: Impacts of Roots
564 Properties and Root Failure Mechanisms. Soil Sci. Soc. Am., 73 (4), 1276-1285.
565 Muukkonen, P. and Makipaa, R., 2004. Biomass equations for european tree:
566 addendum. Silva Fennica, 40 (4), 763-773.
567 Neitsch, S., Arnold, J., Kiniry, J., Williams, J., 2011. Soil and Water Assessment
568 Tool: Theoretical documentation. Water Resources Institute Technical Report No
569 406. Texas, US.
570 Ng., C.W.W., Woon, K.X., Leung, A.K., Chu, L.M., 2013. Experimental
571 investigation of induced suction distribution in grass-covered soil. Ecological
572 Engineering, 52, 219-223.
573 Nordh, N.E. and Verwijst, T., 2004. Aboveground biomass assessments and first
574 cutting cycle production in willow (*Salix* sp.) coppice – a comparison between
575 destructive and non-destructive methods. Biomass Bioenergy, 27, 1-8.
576 Norris, J. S. et al., 2008. Slope Stability and Erosion Control: Ecotechnological
577 Solutions. Springer, Doerdrecht, The Netherlands.
578 Paternoster, R., Brame, R., Mazerolle, P., and Piquerom A. R., 1998. Using the
579 correct statistical test for the equality of regression coefficients. Criminology,
580 36(4), 859-866.
581 Person, G., 1995. Willow stand evapotranspiration simulated for Swedish soils.
582 Agricultural Water Management, 28,271-293.

583 Powel, D., 2005. How to measure a big tree. USDA, Forest Service.
584 Priestley, C., and Taylor, R., 1972. On the Assessment of Surface Heat Flux and
585 Evaporation Using Large-Scale Parameters. Monthly Weather Review. 100 (2),
586 81-92.
587 Raz-Yaseef, N., Rotenberg, E. and Yakir, D., 2010. Effects of spatial variations in soil
588 evaporation caused by tree shading on water flux paeritioning in a semi-arid pine
589 forest. Agricultural and Forest Meteorology, 150, 454-462.
590 Read, D. and Gregory, P.J., 1997. Surface tension and viscosity of axenic maize and
591 lupin mucilages. New Phytologist, 157, 315-326.
592 Read, D., Bengough, A., Gregory, P., Crawford, J., Robinson, D., and Scrimgeour, C.,
593 2003. Plant roots release phospholipid surfactants that modify the physical and
594 chemical properties of soil. New Phytologist, 157, 315-236.
595 Roderick, M.L., Sun, F., Lim, W.H., Farquhar, G.D., 2014. A general framework for
596 understanding the response of the water cycle to global warming over land and
597 ocean. Hydrology and Earth System Sciences, 18(5), 1575-1589.
598 Rodriguez-Iturbe, I. and Porporato, A. 2004. Ecohydrology of Water-Controlled
599 Ecosystems. Cambridge University Press, New York, US.
600 R Core Team, 2015. R: A language and environment for statistical computing. Viena,
601 Austria: R Foundation for Statistical Computing URL: http://www.R-project.org
602 Savabi, M.R. and Williams, J.R., 1995. Water balance and percolation. In: Flanagan,
603 D.C. and Nearing, M.A. (eds), USDA-Water Erosion Prediction Project:
604 Hillslope and watershed model documentation. NSERL Report No. 10.. USDA-
605 ARS National Soil Erosion Research Laboratory, West Lafayette, US.
606 Scanlan, C.A., 2009. Porcesses and effects of root-induced changes to soil hydraulic
607 properties. PhD Thesis, University of Western Australia.

608 Scholl, P., Leitner, D., Kammerer, G., Loiskandl, W., Kaul, H. and Bodner, G., 2014.
609 Root induced changes of effective 1D hydraulic properties in a soil column. Plant
610 Soil. 381:193-213.
611 Shukla, M.J., 2014. Soil Physics. An Introduction. CRC Press, London, UK.
612 Sidle, R.C. and Bogaard, T.A., 2016. Dynamic earth system and ecological controls
613 of rainfall-induced landslides. Earth-Science Reviews, 159, 275-291.
614 Simon, A. and Collison, J., 2002. Quantifying the mechanical and hydrological
615 effects of riparian vegetation on streambank stability. Earth Surface Processes
616 and Landforms, 27, 527-546.
617 Stokes, A., Douglas, G., Fourcaud, T., Giadrossich, F., Gillies, C., Hubble, T., et al.,
618 2014. Ecological mitigation of hillslope instability: ten key issues facing
619 researchers and practitioners. Plant Soil , 377, 1-23.
620 Stokes, A., Norris, J., van Beek, L., Bogaard, T., Cammeraat, E., Mickovski, S., et al.,
621 2008. How vegetation reinforces soil on slopes. In J. Norris, A. Stokes, S.
622 Mickovski, E. Cammeraat, R. van Beek, B. Nicoll, et al., Slope Stability and
623 Erosion Control: Ecotechnological Solutions (pp. 65-116). Springer, Dordrecht,
624 The Netherlands.
625 Tardio, G., Gonzalez-Ollauri, A., Mickovski, S.B., 2016. A non-invasive preferential
626 root distribution analysis methodology from a slope stability apporach.
627 Ecological Engineering, 97, 46-57.
628 Thorne, C.R., 1990. Effects of vegetation on riverbank erosion and stability. In:
629 Thornes, J. B. (Ed.), Vegetation and Erosion (pp. 125-143). John Wiley and Sons
630 Inc., Chichester

631 Vanapalli, S. K., Fredlund, D. G., Pufahl, D. E., Clifton, A. W., 1996. Model for the
632 prediction of shear strength with respect to soil suction. Can. Geotech. J. 33:379-
633 392.
634 van Dijk, A.I.J.M. and Bruijnzeel, L., 2001. Modelling rainfall interception by
635 vegetation of variable density using an adapted anylitical model. Part I: Model
636 description. Journal of Hydrology, 247**,** 230-238
637 van Genuchten, M., 1980. A closed-form equation predicting hydraulic conductivity
638 of unsaturated soils. Soil Sci. Soc. Am. J., 44, 892-898.
639 Vergani, C. and Graf, F., 2016. Soil permeability, aggregate stability and root growth:
640 a pot experiment from a soil bioengineering perspective. Ecohydrology, 9, 830-
641 842.
642 voor de Poorte, P., 2011. Retrieved 7 24, 2015, from PEDROX, live weather from
643 Catterline: http://www.pedrox.com
644 Walker, L. R., Velazquez, E. and Shiels, A.B., 2009. Applying lessons from
645 ecological succession to the restoration fo landslides. Plant Soil, 324, 157-168.
646 Wever, L.A., Flanagan, L.B. and Carlson, P.J., 2002. Seasonal and interannual
647 variation in evapotranspiration, energy balance and surface conductance in a
648 northern temperate grassland. Agricultural and Forest Meteorology, 112, 31-49.
649 Wilkinson, P. L., Anderson, M. G., Lloyd, D. M. 2002. An integrated hydrological
650 model for rain-induced landslide prediction. Earth Surface Processes and
651 Landforms. 27, 1285-1297.
652 Wilkox, R. R. and Keselman, H. J., 2003. Modern robust data analysis methods:
653 measures of central tendency. Psychol. Methods 8(3):254-274.
654 Wu, H. M., 1979. Strength of tree roots and landslides on Prince of Wales Island,
655 Alaska. Canadian Geotechnical Journal. 16 (1), 19-33.

656 Yuan, C., Gao, G., Fu, B., 2016. Stemflow of a xerophytic shrub (*Salix psammophila*)
657 in northern China: Implications for beneficial branch architecture to produce
658 stemflow. Journal of Hydrology. 539, 577-588.
659 Zhang, D-H., Li, X-R., Zhang, F., Zhang, Z-S, Chen, Y-L., 2016. Effects of rainfall
660 intensity and intermittency on woody vegetation cover and deep soil moisture in
661 dryland ecosystems. Journal of Hydrology, 543, 270-282.
662 Zimmermann, A. and Zimmermann, B., 2014. Requirements for throughfall
663 monitoring: The roles of temporal scale and canopy complexity. Agricultural and
664 Forest Meteorology, 189-190, 125-139.
665

FIGURE 1


Catterline Bay
N56.98° E-2.21°
(a)
N
Shallow landslides
North Sea
Scotland
Catterline
0 60 120 Meters
N56.89° E-2.21°
(b)
20 m
UC
LC
UT
LT
10 m
willow-vegetated transect
(c)
fallow transect

666

FIGURE 2

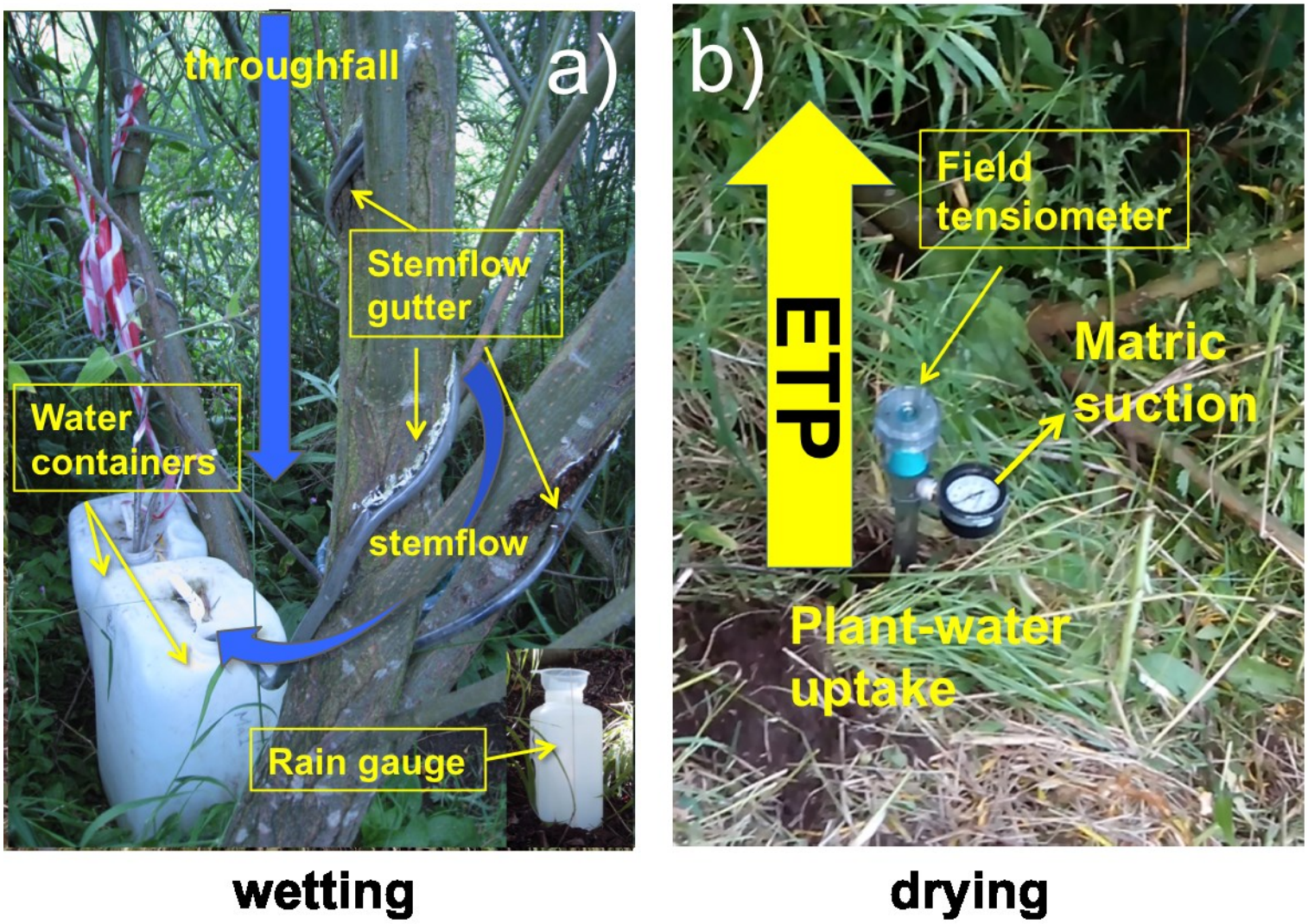
throughfall
a)
Stemflow gutter
Water containers
stemflow
Rain gauge
b)
ETP
Field tensiometer
Matric suction
Plant-water uptake
wetting
drying

667

FIGURE 3

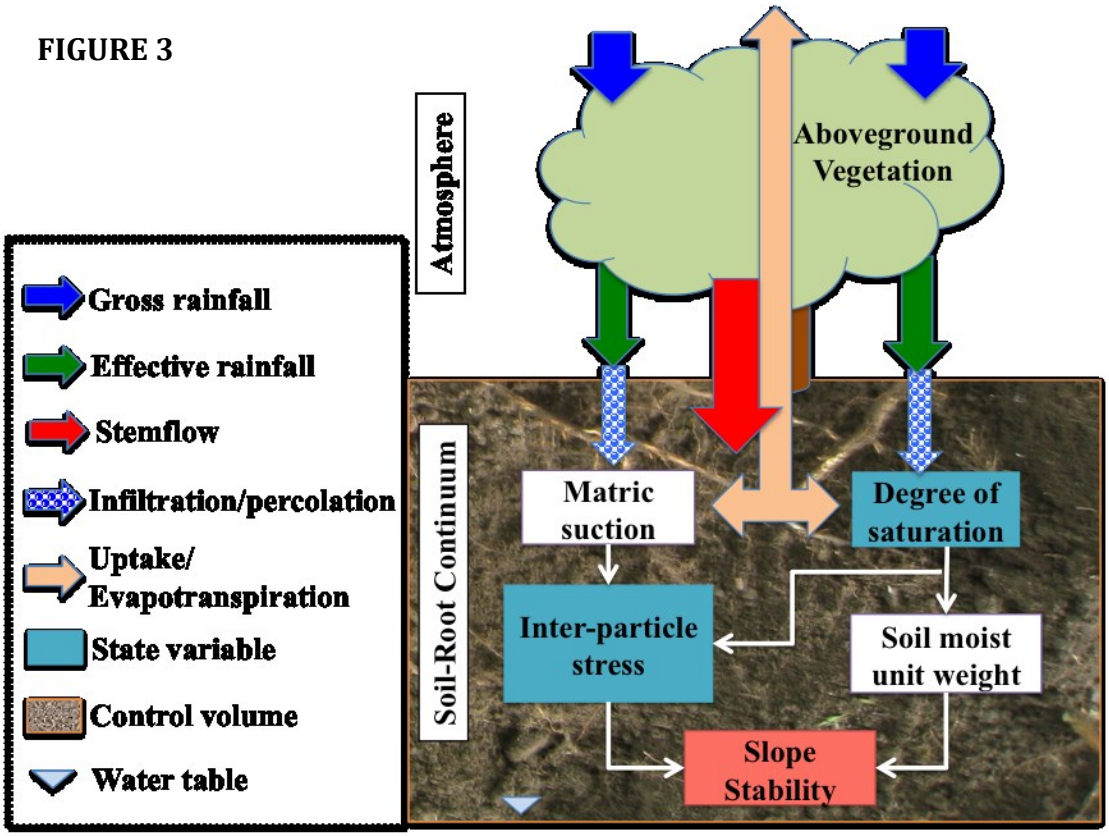
Gross rainfall
Effective rainfall
Stemflow
Infiltration/percolation
Uptake/
Evapotranspiration
State variable
Control volume
Water table
Atmosphere
Aboveground
Vegetation
Soil-Root Continuum
Matric
suction
Degree of
saturation
Inter-particle
stress
Soil moist
unit weight
Slope
Stability

668

FIGURE 4

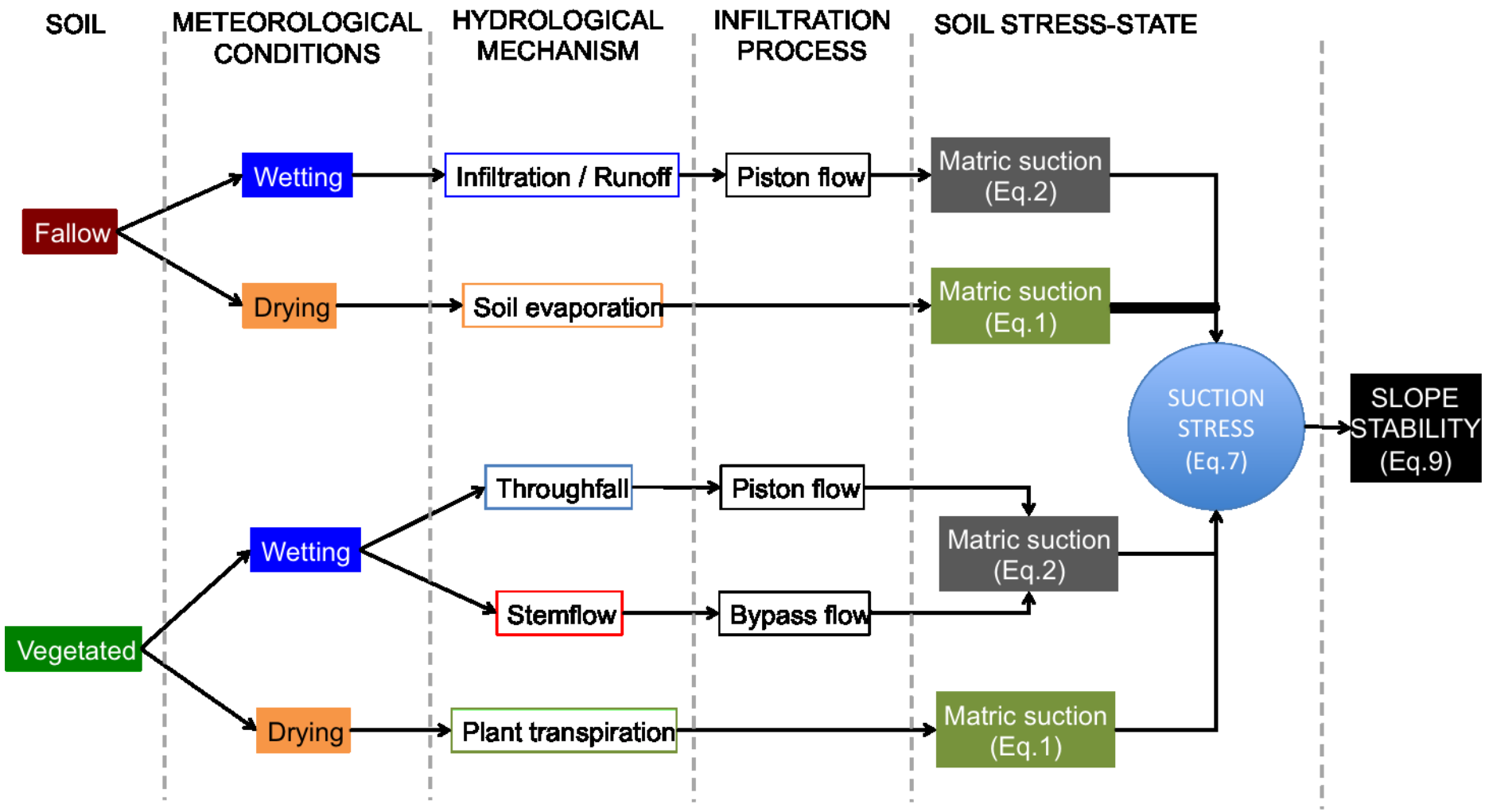
SOIL
METEOROLOGICAL CONDITIONS
HYDROLOGICAL MECHANISM
INFILTRATION PROCESS
SOIL STRESS-STATE
Fallow
Wetting
Drying
Infiltration / Runoff
Soil evaporation
Piston flow
Matric suction (Eq.2)
Matric suction (Eq.1)
Vegetated
Wetting
Drying
Throughfall
Stemflow
Plant transpiration
Piston flow
Bypass flow
Matric suction (Eq.2)
Matric suction (Eq.1)
SUCTION STRESS (Eq.7)
SLOPE STABILITY (Eq.9)

669

670

FIGURE 5

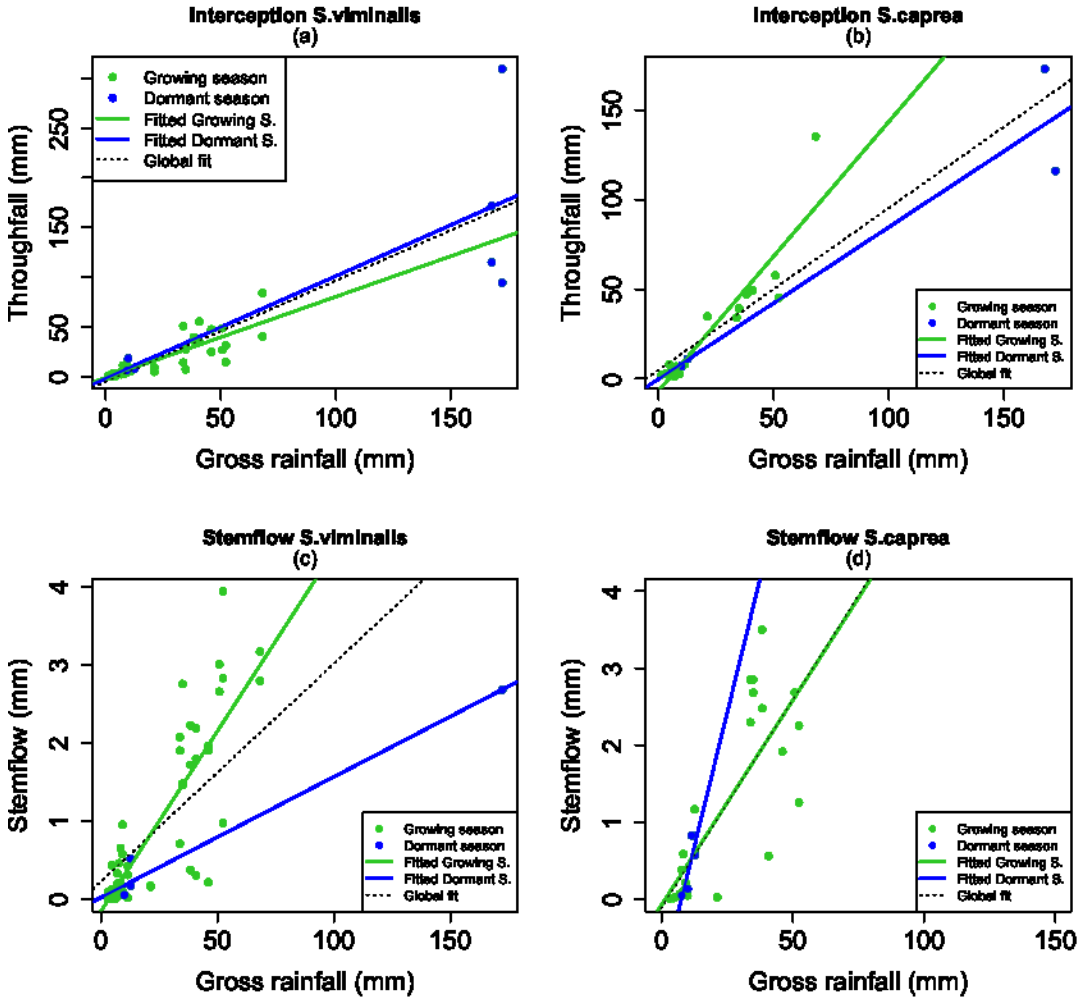
Interception S.viminalis
(a)
Growing season
Dormant season
Fitted Growing S.
Fitted Dormant S.
Global fit
Throughfall (mm)
Gross rainfall (mm)
Interception S.caprea
(b)
Throughfall (mm)
Gross rainfall (mm)
Stemflow S.viminalis
(c)
Stemflow (mm)
Gross rainfall (mm)
Stemflow S.caprea
(d)
Stemflow (mm)
Gross rainfall (mm)

671

672 **FIGURE 6**

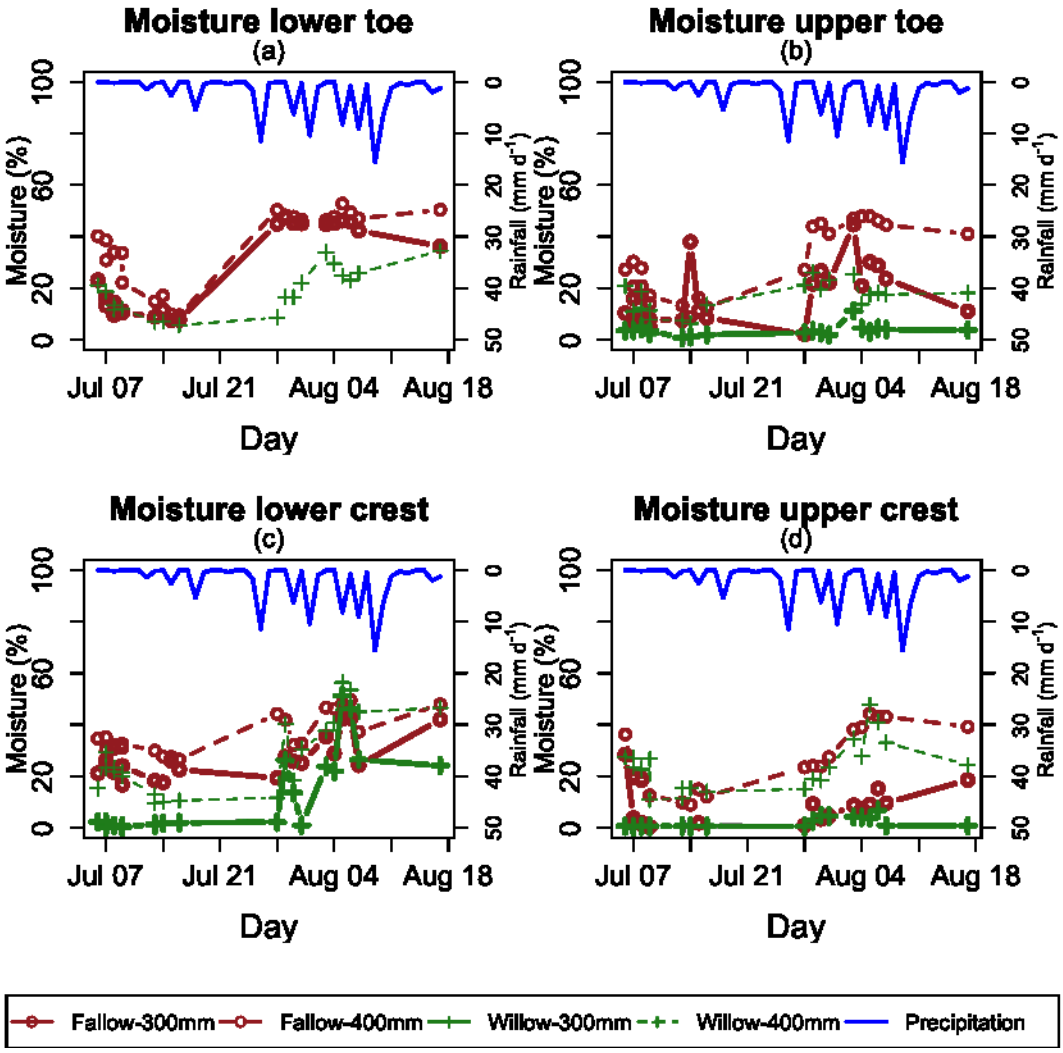

673
674
675
676
677
678
679
680
681

682

FIGURE 7

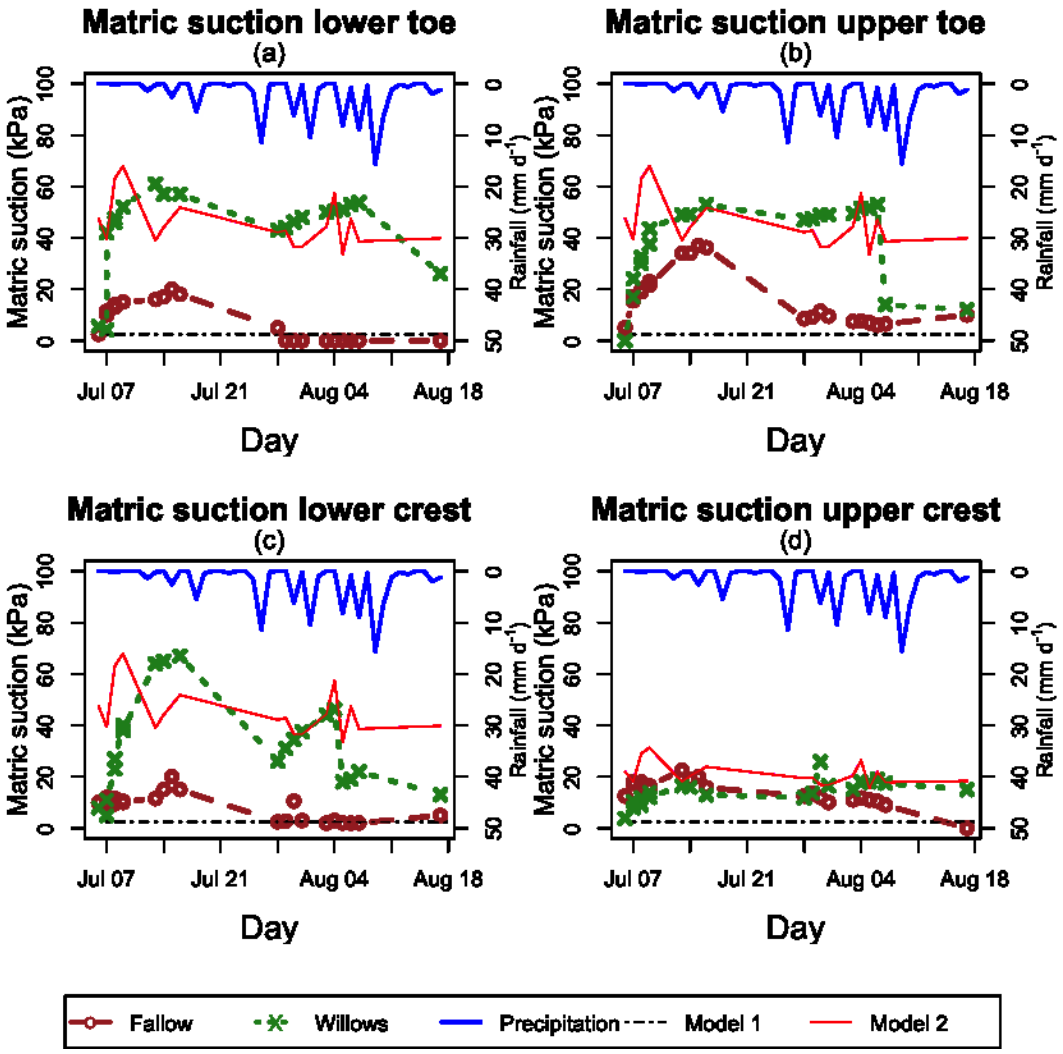
Matric suction lower toe
(a)
Matric suction upper toe
(b)
Matric suction lower crest
(c)
Matric suction upper crest
(d)
Matric suction (kPa)
Rainfall (mm d⁻¹)
Jul 07
Jul 21
Aug 04
Aug 18
Day
Fallow
Willows
Precipitation
Model 1
Model 2

FIGURE 8

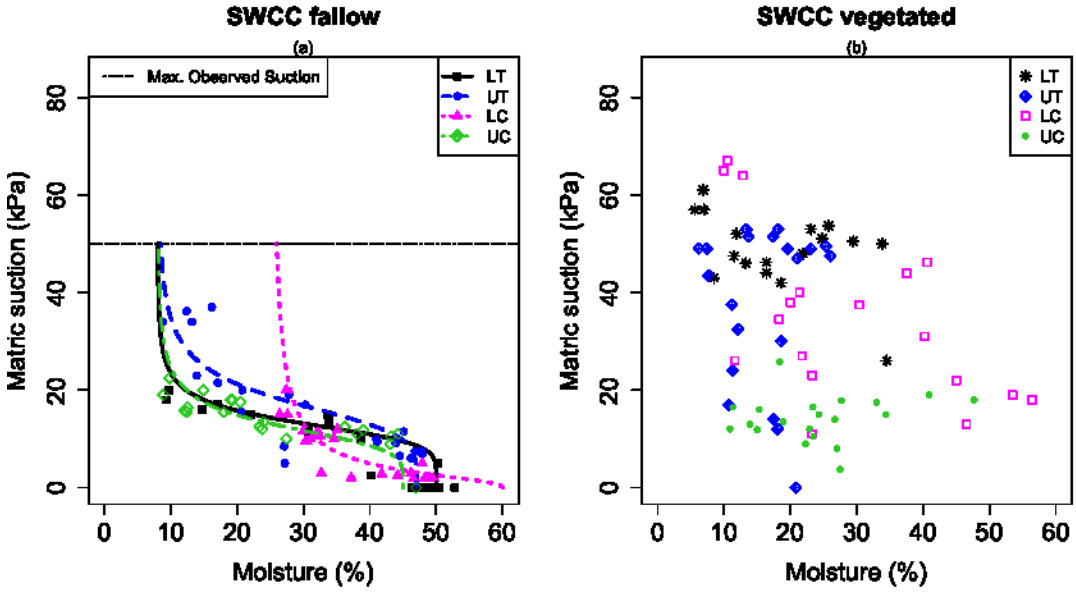
SWCC fallow
(a)
Max. Observed Suction
LT
UT
LC
UC
Matric suction (kPa)
Moisture (%)
SWCC vegetated
(b)
LT
UT
LC
UC
Matric suction (kPa)
Moisture (%)

683

FIGURE 9

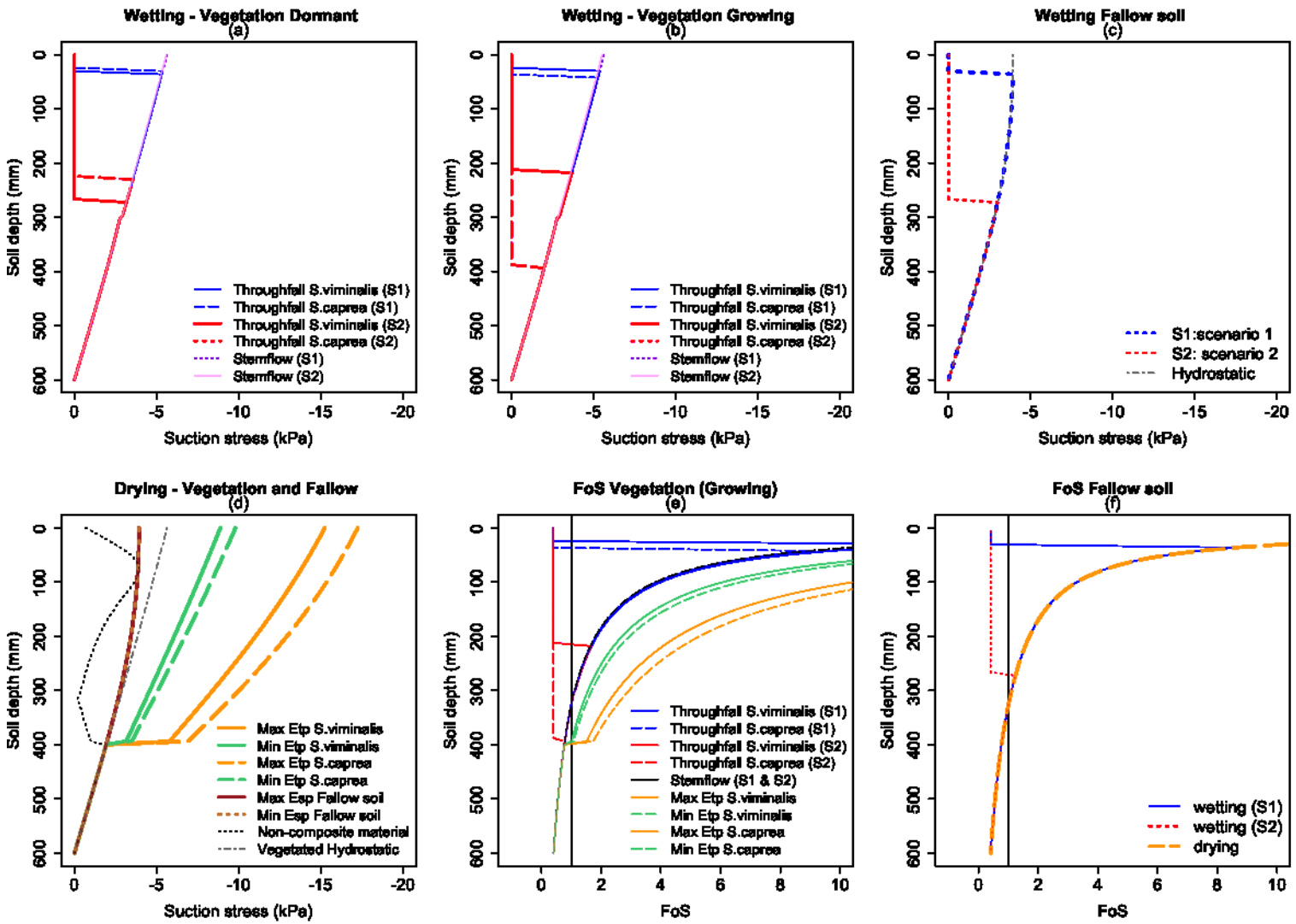
Wetting - Vegetation Dormant
(a)
Soil depth (mm)
Suction stress (kPa)
Throughfall S.viminalis (S1)
Throughfall S.caprea (S1)
Throughfall S.viminalis (S2)
Throughfall S.caprea (S2)
Stemflow (S1)
Stemflow (S2)
Wetting - Vegetation Growing
(b)
Wetting Fallow soil
(c)
S1:scenario 1
S2: scenario 2
Hydrostatic
Drying - Vegetation and Fallow
(d)
Max Etp S.viminalis
Min Etp S.viminalis
Max Etp S.caprea
Min Etp S.caprea
Max Esp Fallow soil
Min Esp Fallow soil
Non-composite material
Vegetated Hydrostatic
FoS Vegetation (Growing)
(e)
Stemflow (S1 & S2)
FoS
FoS Fallow soil
(f)
wetting (S1)
wetting (S2)
drying

684

685